Aus der Klinik für Augenheilkunde
der Medizinischen Fakultät Charité – Universitätsmedizin Berlin

DISSERTATION

Microglia in pathological neovascularization in the retina

zur Erlangung des akademischen Grades
Doctor rerum medicinalium (Dr. rer. medic.)

vorgelegt der Medizinischen Fakultät
Charité – Universitätsmedizin Berlin

von

Sergio Crespo García

aus **Novelda (Spain)**

Datum der Promotion: **10.03.2017**

Table of contents

ABSTRACT (ENGLISH)

INTRODUCTION. Mononuclear phagocytes (e.g. microglia, macrophages) have been characterized as potential mediators of retinal neovascularization and degeneration. *In vivo* assessments of mononuclear phagocyte behavior in animals provides an important insight into disease that improves the understanding of pathological mechanisms and helps to approach new therapy developments. Conventional scanning laser ophthalmoscope (SLO), a widely used clinical tool, also permits to track GFP-positive mononuclear phagocytes in specific transgenic animal models. In this work we validate conventional SLO imaging as a tool capable to characterize the spatial- and time-dependent course of mononuclear phagocyte activation in MacGreen mice undergoing laser-induced choroidal neovascularization (CNV). This is a standardized experimental procedure to mimic the neovascularization that occurs in wet age-related macular degeneration.

METHODS. Using argon laser, CNV was induced in MacGreen mice. Transgenic MacGreen mice harbor a myeloid-promotor driven GFP-expression that allows monitoring of mononuclear phagocytes *in vivo* by means of fundus auto-fluorescence in SLO. Data was verified *ex vivo* using retinal flat-mount preparations or sagittal sections.

RESULTS. Mononuclear phagocytes were characterized in different morphological subsets regarding their activation state (e.g. round shape as activated state, ramified processes as surveying) and detected in the inner and outer plexiform layers of the retina. *In vivo* imaging permitted to quantify spatial and temporal distribution of activated and surveying GFP-positive cells during a time-course after CNV induction. The maximum number of activated cells was detected at day 4 after laser treatment in the inner plexiform layer. Immediately after laser, no acute activation was detected. Furthermore, the spatial distribution of the activation changed by the time in the inner retina. Significant time and spatial changes were not shown in the outer layer. When doubling the laser power impact, the number of activated GFP-positive cells was not significantly increased.

CONCLUSIONS. Thus conventional SLO proves to be suitable for an *in vivo* read-out and quantification of mononuclear phagocyte activation. Data showed that laser damage at the outer retina led to more mononuclear phagocyte activity in the inner retina independent of laser power. Findings regarding the spatial distribution of activated cells unveil a new perspective in

the understanding of the cellular immune response in the retina *in vivo*. After this methodological evaluation, we are currently exploring the same model by hypothesis-driven interventional studies (e.g. intravitreal injections treatment) or in other retinal disease conditions such as oxygen-induced retinopathy, which emulates pre-retinal neovascularization, and streptozotocin-induced type 1 diabetes, as a model for experimental diabetic retinopathy.

ABSTRACT (GERMAN)

EINLEITUNG. Mononukleäre Phagozyten (z.B. Microglia, Macrophagen) wurden als mögliche Vermittler von retinaler Gefäßneubildung und Degeneration identifiziert. Tierexperimentelle Krankheitsmodelle ergeben zusammen mit *in vivo* Untersuchungen wichtige Einblicke in korrespondierende Erkrankungen und sind im besonderen Maße wertvoll sowohl für die Entwicklung von Therapien als auch für das Verständnis zu Grunde liegender Pathomechanismen. Konventionelle Scanning Laser Ophthalmoskopie (SLO), eine in der Klinik weit verbreitete Methode, erlaubt es auch GFP-positive mononukleäre Phagozyten in bestimmten transgenen Tieren zu detektieren. In dieser Doktorarbeit validieren wir *in vivo* Bildgebung mittels konventioneller SLO als adäquates Verfahren, den räumlichen und zeitlichen Verlauf der Aktivierung mononukleärer Phagozyten in MacGreen Mäusen nach Laser induzierter chorioidaler Neovaskularisation (CNV) darzustellen. Dabei handelt es sich um ein standardisiertes experimentelles Vorgehen um Neovaskularisation bei feuchter altersbedingter Makuladegeneration zu simulieren.

METHODEN. CNV wurde in MacGreen Mäusen mittels Argonlaser induziert. Transgene MacGreen Mäuse zeigen eine für myeloische Zellen spezifische GFP Expression, welche die Beobachtung mononukleärer Phagozyten *in vivo* mittels Fundusautofluoreszenz ermöglicht. Die *in vivo* Daten wurden *ex vivo* in retinalen Flachpräparaten und Sagittalschnitten verifiziert.

ERGEBNISSE. Mononukleäre Phagozyten wurden hinsichtlich ihres Aktivierungsgrades in morphologische Gruppen unterteilt (z.B. runde Form als aktivierter Zustand, Form mit ramifizierten Fortsätzen als „überwachende“ Form) und in der inneren und äußeren Retina delektiert. Die *in vivo* Bildgebung erlaubte die räumliche und zeitliche Verteilung der aktivierten und „überwachenden“ GFP-positiven Zellen nach der Laser-Behandlung zu quantifizieren. Das Maximum aktivierter Zellen wurde an Tag 4 nach Laser in der inneren plexiformen Schicht delektiert. Es kam zu keiner akuten Aktivierung direkt nach der Laserintervention. Des Weiteren veränderte sich die räumliche Verteilung der Zellaktivierung in der inneren Retina über die Zeit. In der äußeren Schicht kam es zu keinerlei signifikanten Veränderungen. Eine Verdopplung der Laserleistung führte nicht zu einem signifikanten Anstieg aktivierter GFP-positiver Zellen.

SCHLUSSFOLGERUNG. Somit ist konventionelles SLO geeignet für die *in vivo* Quantifizierung der Aktivierungsmuster mononukleärer Phagozyten. Unsere Daten zeigen, dass der Schaden durch den Laser in der äußeren Retina zu vermehrter Aktivierung mononukleärer Phagozyten in der inneren Retina führte, unabhängig von der Laserleistung. Des Weiteren wird eine neue Perspektive auf das Verständnis der Immunantwort in der Retina *in vivo* eröffnet. Nach dieser methodischen Evaluation untersuchen wir zur Zeit am selben Modell Hypothesen-getriebene interventionelle Ansätze (z.B. intravitreale Injektionen) im Zusammenhang mit anderen gefäßspezifischen und/oder neurodegenerativen Entitäten, wie z.B. Sauerstoff induzierter Retinopathie, welche präretinale Neovaskularisation simuliert, oder Streptozotocin induzierter Typ 1 Diabetes als experimentelles Modell für diabetische Retinopathie.

Affidavit

I, **Sergio Crespo García**, certify under penalty of perjury by my own signature that I have submitted the thesis on the topic **"Microglia in pathological neovascularization in the retina"**. I wrote this thesis independently and without assistance from third parties, I used no other aids than the listed sources and resources.

All points based literally or in spirit on publications or presentations of other authors are, as such, in proper citations (see "uniform requirements for manuscripts (URM)" the ICMJE www.icmje.org) indicated. The sections on methodology (in particular practical work, laboratory requirements, statistical processing) and results (in particular images, graphics and tables) correspond to the URM (s.o) and are answered by me. My contributions in the selected publications for this dissertation correspond to those that are specified in the following joint declaration with the responsible person and supervisor. All publications resulting from this thesis and which I am author of correspond to the URM (see above) and I am solely responsible.

The importance of this affidavit and the criminal consequences of a false affidavit (section 156,161 of the Criminal Code) are known to me and I understand the rights and responsibilities stated therein.

Date 20.05.2016 Signature

Declaration of any eventual publications

Sergio Crespo García had the following share in the following publication:

Publication 1: **Crespo-Garcia S**, Reichhart N, Hernandez-Matas C, Zabulis X, Kociok N, Brockmann C, Joussen AM, Strauss O. In vivo analysis of the time and spatial activation pattern of microglia in the retina following laser-induced choroidal neovascularization. *Experimental Eye Research* 139:13-21, **2015**

Contribution in detail: Sole first authorship. Experimental design; execution of all animal experiments *in vivo* (animal breeding, laser-induced choroidal neovascularization and subsequent imaging using scanning laser ophthalmoscope) and *ex vivo* (immunodetection in retinal sagittal sections and flat-mount preparations and staining); microscopy; data analysis and interpretation. Manuscript writing (including figures) and revision.

Signature, date and stamp of the supervising University teacher

Signature of the doctoral candidate

ISI Web of Knowledge℠

Journal Citation Reports®

WELCOME HELP

2014 JCR Science Edition

Journal Summary List

Journal Title Changes

Journals from: subject categories OPHTHALMOLOGY VIEW CATEGORY SUMMARY LIST

Sorted by: Impact Factor SORT AGAIN

Journals 1 - 20 (of 57) [1 | 2 | 3] **Page 1 of 3**

MARK ALL UPDATE MARKED LIST

Ranking is based on your journal and sort selections.

Mark	Rank	Abbreviated Journal Title (linked to journal information)	ISSN	JCR Data						*Eigenfactor*® Metrics	
				Total Cites	Impact Factor	5-Year Impact Factor	Immediacy Index	Articles	Cited Half-life	*Eigenfactor*® Score	*Article Influence*® Score
☐	1	PROG RETIN EYE RES	1350-9462	4326	8.733	10.439	1.828	29	7.6	0.00908	3.688
☐	2	OPHTHALMOLOGY	0161-6420	29035	6.135	6.117	1.581	313	8.3	0.05029	1.851
☐	3	ARCH OPHTHALMOL-CHIC	0003-9950	17678	4.399	4.372		0	>10.0	0.01844	1.593
☐	4	AM J OPHTHALMOL	0002-9394	20393	3.871	4.225	0.938	323	9.8	0.02767	1.337
☐	5	SURV OPHTHALMOL	0039-6257	4277	3.849	3.712	0.357	56	>10.0	0.00411	1.203
☐	6	J REFRACT SURG	1081-597X	3710	3.468	3.146	0.573	117	5.7	0.00904	0.943
☐	7	INVEST OPHTH VIS SCI	0146-0404	44803	3.404	3.673	0.617	969	7.6	0.07624	0.996
☐	8	OCUL SURF	1542-0124	944	3.341	3.667	0.955	22	7.3	0.00129	0.966
☐	9	JAMA OPHTHALMOL	2168-6165	734	3.318	3.318	0.868	174	1.4	0.00335	1.219
☐	10	RETINA-J RET VIT DIS	0275-004X	7270	3.243	3.121	0.745	290	5.3	0.01658	0.863
☐	11	BRIT J OPHTHALMOL	0007-1161	15920	2.976	2.861	0.714	322	9.8	0.02272	0.923
☐	12	ACTA OPHTHALMOL	1755-375X	5671	2.844	2.513	0.537	229	7.1	0.01036	0.681
☐	13	J CATARACT REFR SURG	0886-3350	10699	2.722	2.803	0.552	277	7.2	0.01773	0.744
☐	14	EXP EYE RES	0014-4835	9517	2.709	3.023	0.542	238	8.6	0.01443	0.868
☐	15	CURR OPIN OPHTHALMOL	1040-8738	2432	2.500	2.688	0.423	78	6.8	0.00542	0.887
☐	16	J VISION	1534-7362	8027	2.393	3.113	0.416	269	5.4	0.02660	1.140
☐	17	CLIN EXP OPHTHALMOL	1442-6404	2459	2.347	2.140	0.621	87	6.0	0.00605	0.691
☐	18	VISUAL NEUROSCI	0952-5238	2752	2.207	2.166	0.667	33	>10.0	0.00235	0.909
☐	19	OPHTHAL PHYSL OPT	0275-5408	2054	2.177	1.801	0.946	56	9.4	0.00311	0.527
☐	20	J GLAUCOMA	1057-0829	2930	2.106	1.993	0.360	150	6.7	0.00540	0.575

MARK ALL UPDATE MARKED LIST

Journals 1 - 20 (of 57) [*1* | 2 | 3] **Page 1 of 3**

THOMSON REUTERS

Published by Thomson Reuters

Experimental Eye Research 139 (2015) 13–21

Contents lists available at ScienceDirect

Experimental Eye Research

journal homepage: www.elsevier.com/locate/yexer

In vivo analysis of the time and spatial activation pattern of microglia in the retina following laser-induced choroidal neovascularization

Sergio Crespo-Garcia [a], Nadine Reichhart [a], Carlos Hernandez-Matas [b, c], Xenophon Zabulis [b], Norbert Kociok [a], Claudia Brockmann [a], Antonia M. Joussen [a], Olaf Strauß [a, *]

[a] Department of Ophthalmology, Charité University Medicine Berlin, Berlin, Germany
[b] Institute of Computer Science, Foundation for Research and Technology – Hellas, Heraklion, Greece
[c] Computer Science Department, University of Crete, Heraklion, Greece

ARTICLE INFO

Article history:
Received 8 February 2015
Received in revised form
14 July 2015
Accepted in revised form 22 July 2015
Available online 26 July 2015

Keywords:
MacGreen mice
Macrophages and microglia cells
Amoeboid
In vivo imaging
CNV

ABSTRACT

Microglia play a major role in retinal neovascularization and degeneration and are thus potential targets for therapeutic intervention. *In vivo* assessment of microglia behavior in disease models can provide important information to understand patho-mechanisms and develop therapeutic strategies. Although scanning laser ophthalmoscope (SLO) permits the monitoring of microglia in transgenic mice with microglia-specific GFP expression, there are fundamental limitations in reliable identification and quantification of activated cells. Therefore, we aimed to improve the SLO-based analysis of microglia using enhanced image processing with subsequent testing in laser-induced neovascularization (CNV).

CNV was induced by argon laser in MacGreen mice. Microglia was visualized *in vivo* by SLO in the fundus auto-fluorescence (FAF) mode and verified *ex vivo* using retinal preparations.

Three image processing algorithms based on different analysis of sequences of images were tested. The amount of recorded frames was limiting the effectiveness of the different algorithms. Best results from short recordings were obtained with a pixel averaging algorithm, further used to quantify spatial and temporal distribution of activated microglia in CNV. Morphologically, different microglia populations were detected in the inner and outer retinal layers. In CNV, the peak of microglia activation occurred in the inner layer at day 4 after laser, lacking an acute reaction. Besides, the spatial distribution of the activation changed by the time over the inner retina. No significant time and spatial changes were observed in the outer layer. An increase in laser power did not increase number of activated microglia.

The SLO, in conjunction with enhanced image processing, is suitable for *in vivo* quantification of microglia activation. This surprisingly revealed that laser damage at the outer retina led to more reactive microglia in the inner retina, shedding light upon a new perspective to approach the immune response in the retina *in vivo*.

1. Introduction

The activation of macrophages plays an important role in the pathology of AMD. From their origin, these can be resident macrophages such as dendritic cells or microglia as well as systemic macrophages invading the area of tissue damage and stimulate VEGF-A secretion by the retinal pigment epithelium (Grisanti and Tatar, 2008; Witmer et al., 2003). However, the functional phenotype of macrophages seems to be more important than their origin. The functional phenotyping of macrophages has gained more and more attention in the analysis of patho-mechanisms in the retina and has overcome the classic M1/M2 classification (Chambers et al., 2013; Murray et al., 2014). Recent data suggest that activation of microglia cells in the retina might play a central role in the coordination of pathological events including neovascularization (Eter et al., 2008). Investigation of microglia behavior in mouse models for inherited retinal degeneration revealed that microglia becomes active already before first pro-apoptotic genes are up-

* Corresponding author. Department of Ophthalmology, Charité Universitätsmedizin Berlin, Campus Virchow Klinikum, Augustenburger Platz 1, 13353 Berlin, Germany.
E-mail address: olaf.strauss@charite.de (O. Strauß).

http://dx.doi.org/10.1016/j.exer.2015.07.012
0014-4835/

regulated (Stoecker et al., 2009). Under subtle changes in the retina, microglia cells seem to be one of the cell populations to preserve its integrity. Thus regulation of microglia activity represents an ideal target to develop strategies to prevent retinal degeneration and likely neovascularization at very early stages of the disease.

Translational research depends on identification of pathomechanisms *in vivo* and precise follow-up of disease progression. The first is important because the complexity of an organism cannot be simulated in cell culture, but is required for development of therapeutic strategies. The latter is essential to define time points for intervention and to precisely monitor possible beneficial effects. Some animal models, combined with refinement of clinical imaging tools that are commonly used for AMD patients, enable analysis of cellular and molecular events non-invasively and in real-time. These models reduce significantly the amount of animals needed for experimentation and increase the reliability of the data in terms of translational medicine (Contag and Bachmann, 2002; Edinger et al., 2002; Rudin and Weissleder, 2003). In order to define a strategy to inhibit microglia activation as therapeutic target, the accurate knowledge on time-dependence macrophage activation, their spatial distribution and their phenotypes *in vivo* is needed. This kind of data can be obtained by using transgenic mice expressing a microglia/macrophage-specific fluorescence reporter. MacGreen mice specifically expressing EGFP in macrophages, mouse models with injected GFP-positive bone marrow cells (chimeric model) or the CX3CR1$^{GFP/+}$ knock-in mice, in which GFP expression is under control of the fractalkine receptor CX3CR1, are the most commonly used animal models for this purpose (Eter et al., 2008; Joly et al., 2009; Muther et al., 2010; Sasmono et al., 2003). In these mouse models, microglia can be visualized by their GFP fluorescence using scanning laser ophthalmoscopy (SLO). The active microglia can be roughly identified by their change in cell morphology from ramified surveying phenotype to the amoeboid invading one. However, the resolution must be high enough to permit a clear and valid identification and separation between active and surveying microglia. Using a confocal SLO, Alt and colleagues (Alt et al., 2014) obtained images which provide the required resolution to safely identify activated microglia and could even establish automated counting of the activated cells. When using conventional SLO, which is also used in the clinic to permit an easy translation of the data from animal model to patients, the raw output doesn't have a high enough resolution for a valid discrimination between surveying and active cells. For example Eter and colleagues (Eter et al., 2008) could visualize the microglia by conventional SLO, but were relying on FACS analysis for their quantification.

In summary, recent publications demonstrated the need and the feasibility of *in vivo* techniques for translational research in retinal degeneration. The combination of transgenic mouse models and standard SLO was shown to permit *in vivo* analysis of cellular immune responses in retinal degenerations. However, using a conventional SLO, the output resolution is too poor to obtain a complete description of the cellular immune response in terms of a reliable *in vivo* quantification as well as spatial and temporal distribution patterns. Thus, the aim of the study is to improve SLO-based *in vivo* imaging to obtain such a complete assessment. We used laser-induced CNV in MacGreen mice to mimic the most threatening AMD complication, and analyzed the spatial and temporal behavior of microglia with a conventional SLO. By comparing several algorithms for enhanced image analysis, we not only established a method for quantification of microglia activation for translational purposes, but also discovered new aspects of microglia behavior in laser-induced CNV.

2. Methods

2.1. Animal model

B6N.Cg-Tg(Csf1r-EGFP)1Hume/J mice, commonly referred as MacGreen transgenic mice, were kindly provided by H. Kettenmann (Max-Delbrück-Center for Molecular Medicine, Berlin, Germany). MacGreen mice express enhanced green fluorescent protein in macrophages and trophoblast cells by using the transgene reporter EGFP under the control of Csf1r promoter (Sasmono et al., 2003). C57/Bl6J mice purchased from Janvier (Cedex, France) were used as negative controls for GFP detection. All mice were 10–12 weeks old and weighed over 20 g at the time of the experiment. All animal experiments complied with the guidelines of the ARVO Statement for the Use of Animals in Ophthalmic and Vision Research and were approved by the local governmental authorities (Landesamt für Gesundheit und Soziales, LaGeSo, Berlin).

2.2. Laser-induced choroidal neovascularization

Mice pupils were dilated using tropicamide eye drops before being anesthetized with 1% ketamine hydrochloride (Actavis, München, Germany) and 0.1% xylacine (Rompun, Bayer Vital GmbH, Leverkusen, Germany) in a concentration of 0.1 ml/10 mg bodyweight. CNV was induced by an argon ion laser using the following parameters: either 120 mW (low power) or 240 mW (high power) for 0.1 s, 50 μm spot diameter. Three distinct laser spots were performed in one hemisphere of the fundus, avoiding the large vessels. The appearance of a bubble confirmed the rupture of the Bruch's membrane. Fluorescence angiography (FA) and OCT scanning verified the development of the CNV (Semkova et al., 2014).

2.3. SLO imaging

Pupil dilatation and anesthesia were performed as it has been described above at the laser-induced CNV paragraph. The imaging protocol was conducted using Spectralis HRA-OCT (Heidelberg Engineering, Heidelberg, Germany) (GmbH, 2007). The conventional scanner laser ophthalmoscope (SLO) was used at high resolution mode with an objective adapted for rodents. The maximum scan depth of the setup was 8 mm. All eyes were scanned at different time-points after laser (D0, D1, D4, D7, D14). Scanning was performed with the optic nerve head (ONH) positioned in the center of the image field. Near-infrared reflectance (IR; diode laser, wavelength 820 nm) and OCT scanning pictures were obtained using a mean automatic real time of 30 frames, while autofluorescence imaging (FAF, solid state laser, wavelength 488 nm) was displayed by recording videos from 5 to 15 s with a mean automatic real time of 5 frames focusing on two differentiated layers: inner and outer.

In the healthy retina, the localization of the inner plexiform layer (Focus A, IPL) of microglia can be accomplished by starting with the visualization of larger blood vessels as first orientation point (Fig. 2B, left and central panels); the second layer can be visualized by adjusting the focus with the knob from that level into deeper layers (Focus B, outer plexiform layer or OPL), where autofluorescent ramified microglia appear in a distinct position from the previous one (Fig. 2B, left and right panels). Using ramified microglia to assess the focus has a main advantage: Ramified microglia are exclusively residential and not migrating macrophages, and therefore, a reliable indicator of the layers where they are located. After laser injury we used the untreated area of the retina to position the focus into the Focus A and further assess the Focus B from that.

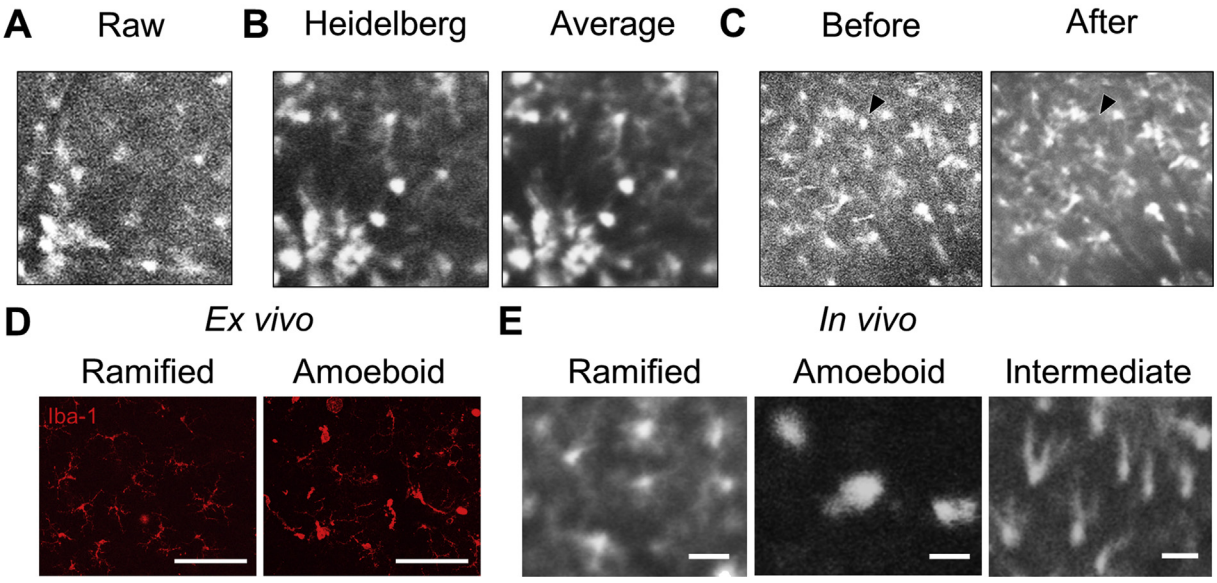

Fig. 1. Identification of Activated Microglia and Image Processing. A (Raw) depicts a video frame from a SLO auto-fluorescence recording obtained roughly. B Comparison of the different output images from the same recorded eye: (Heidelberg) when averaging through the SLO setup option, (Average) applying frame averaging post-recording. C Result of a before (left) and after (right) processed video with the averaging method to reduce the impact of mobile and transient elements, as well as noise. Black arrowhead indicates the position of a transient element before and after processing. D Staining of retina whole-mount against Iba-1 (red) showing different mononuclear phagocyte populations *ex vivo*: on the left, ramified-like and amoeboid-like in the right. Scale bar represents 100 μm. E Magnification of SLO auto-fluorescence image representing the different populations of mononuclear phagocyte *in vivo*: on the left, ramified, on the middle, amoeboid and on the right, an intermediate transient state. Scale bar represents 100 μm.

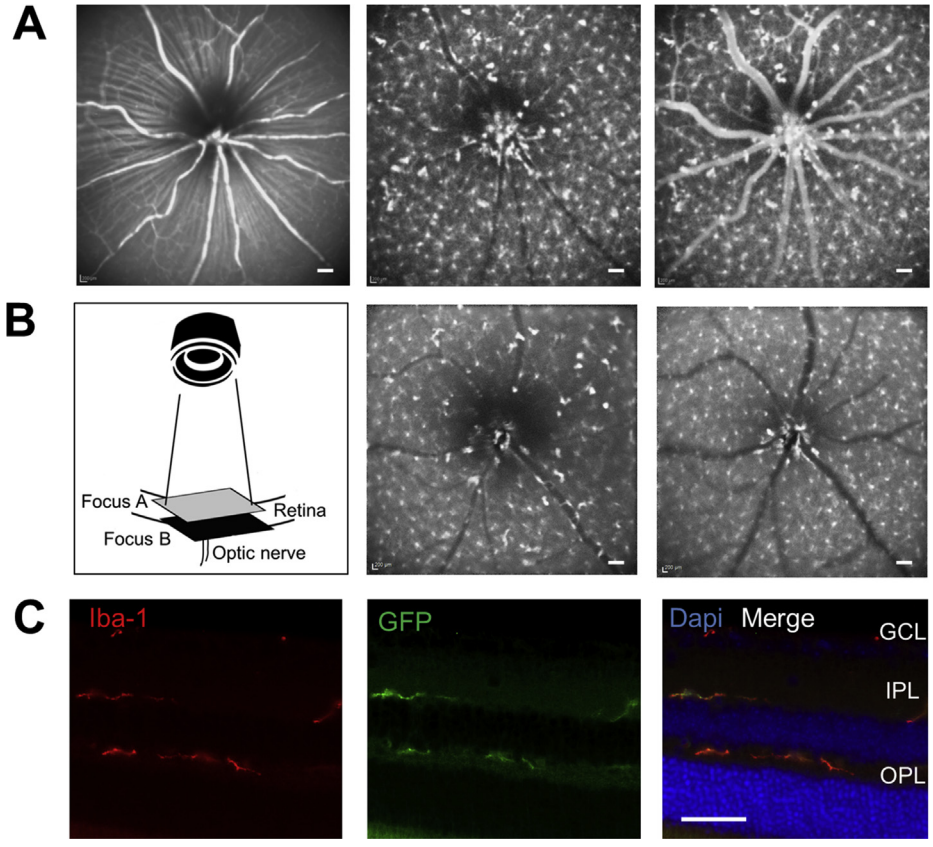

Fig. 2. Identification of Macrophages in Different Retinal Layers. A Left panel: Scanning laser ophthalmoscope (SLO) near-infrared reflectance (IR) image of a control MacGreen mouse. Central panel: SLO auto-fluorescence image showing EGFP fluorescent macrophages due to the transgenic background. Right panel: Fluorescence angiography (FA) illustrating the retinal vessels and the auto-fluorescent signal from macrophages. Scale bar represents 100 μm. B Left panel: Schematic illustration of the focusing technique used at SLO to distinguish the two layers of fluorescent macrophages: Focus A in the inner retina and Focus B in the outer. Central and right panel: SLO auto-fluorescence images matching with the Focus A, assigned as the inner plexiform layer (IPL; central panel) and Focus B, or outer plexiform layer (OPL; right panel). Scale bar represents 100 μm. C Paraffin section of a MacGreen retina reveals merging of Iba-1 reactivity (red) in macrophage auto-fluorescent signal (green). Nuclei were counterstained by DAPI (blue). Scale bar represents 100 μm.

Mentioned FAF measurements were complemented with fluorescence angiography (FA). Images were reviewed and analyzed using Heidelberg Eye Explorer 1.7.0.0. software. Image J 1.44p software (NIH, USA) was used for calculating the percentage of scar auto-fluorescent tissue in FAF images. We considered as scar tissue the auto-fluorescent area which appears on the laser spots in the outer focus, where the laser has a higher impact (Supp. Fig. 1A–B).

2.4. Image processing

The data is composed by grayscale videos acquired with a Spectralis HRA-OCT in the fundus FAF recording mode, with variable duration and a resolution of 496 × 596 pixels.

To reduce the impact of some of the transient components of the image as well as noise, and to obtain a clearer image for the quantification, image processing was applied.

Several techniques were compared. Besides offline frame averaging, the temporal median filter (Huang, 1981) and Rosseeuw's Least Median of Squares (LMedS) (Rousseeuw and Leroy, 1984) were tested in search of a more robust result, protected against intensity outliers. Due to the small number of frames in the videos, the impact of the statistical advantages of these methods was minute as results were numerically equivalent to offline frame averaging.

As it will be discussed later, the frame averaging technique appeared to be best applicable for further *in vivo* analysis. With this method, images in which the value of each pixel is the average value of that pixel for each frame of the video, were produced as indicated by:

$$I(x,y) = \frac{\sum_{i=1}^{n} I_i(x,y)}{n}$$

where $I(x,y)$ is the intensity of the pixel at the coordinates (x,y) of the resulting image, n is the amount of frames in a video and $I_i(x,y)$ is the intensity of the pixel at the coordinates (x,y) of the i-th frame of the video.

In the temporal median filter (Huang, 1981), the value of each pixel is the median value of that pixel for each frame of the video.

$$I(x,y) = \mathrm{med}(\forall i \in n : I_i(x,y))$$

In Rousseeuw's LMedS (Rousseeuw and Leroy, 1984), the intensity value that minimizes the median of the residuals is calculated such that:

$$\mathrm{I}(\mathrm{x},\ \mathrm{y}) = \min_{\mathrm{I_i(x,y)}} \mathrm{med}\, \mathrm{r_i^2}\ \ \forall \mathrm{i} \in \mathrm{n} : \mathrm{I_i(x,y)}$$

The software implementation of the image processing algorithms was developed by the authors in the C++ programming language, following the equations that describe each of them.

2.5. In vivo quantification of microglia

For determination of the microglia activation status as well as their temporal and spatial activation pattern, it is crucial to differentiate between surveying and activated microglia. This is possible by their morphological switch between ramified and amoeboid phenotype (Hanisch and Kettenmann, 2007; Langmann, 2007; Xu et al., 2007). This differentiation was applied in the following way: a.) non-activated cells: the soma of the cell is small in association with multiple prolonged ramifications (Fig. 1D, left panel); b.) activated cells: the soma of the cell is rounded (amoeboid) with no ramifications (Fig. 1D, mid panel); c.) cells with transitory phenotype between resting and activated status: the soma is prominently rounded with still few and thick ramifications (here referred as intermediate, Fig. 1D, right panel).

For the analysis, the fundus of each eye was divided in two equal parts, separating the side with laser spots from the opposite untreated side. Blinded counting was performed by observer for each SLO auto-fluorescence picture (total area of the visual field imaged: 0.7 mm^2) at the two layers imaged at several time points.

2.6. Immunohistochemistry on paraffin sections

Eyes were enucleated at different time-points after laser (D1, D4, D7, D14), fixated in Davidson fixative and embedded in paraffin. Sections of 5 μm thickness were deparaffinized and heat mediated antigen retrieval was performed using TBS-Triton 0.4% (pH = 9). After blocking the sections with 5% BSA they were incubated with a solution containing antibodies against ionized calcium-binding adapter molecule 1 (Iba-1, rabbit polyclonal, 1:500, WAKO chemicals, Richmond, VA) and against GFP (goat polyclonal FITC-conjugated, 1:250, Abcam, Cambridge, UK) over night at 4 °C. Species appropriate secondary antibody for Iba-1 (goat anti rabbit Texas Red, 1:2000, Invitrogen, Karlsruhe, Germany) was applied for 1 h at room temperature and nuclei were counterstained using DAPI (3 μM, Invitrogen). Sections were subjected to an Axio Imager M2 fluorescence microscope (Zeiss, Jena, Germany) and data was analyzed by ZEN lite 2012 Software (Zeiss).

2.7. Preparation and visualization of eye whole-mounts

Eyes were enucleated and fixated in PFA 4% solution for 13 min at RT. Cornea was dissected with a circumferential limbal incision, followed by removal of the lens and vitreous. 4 radial cuts were needed to flatten the eye cup and divide it into two parts by sectioning the optic nerve: the neural retina and the sclera containing the choroid. Retina and sclera were incubated separately over night at 4 °C in a permeabilization solution containing 5% Triton X-100 and incubated in a blocking solution containing 5% BSA for 1 h. For staining the microglia, anti Iba-1 (WAKO) staining was performed as described in the paraffin section. Mononuclear phagocytes were stained using anti-CD11b (anti-ITGAM, 1:100, antibodies-online GmbH, Atlanta, USA); specie secondary antibody was Cy3-conjugated goat anti-rat (1:200, Dianova GmbH, Hamburg, Germany). Blood vessels were visualized using Isolectin B4 – AlexaFluor488 (1:200, Invitrogen). Same procedure applied for the sclera. Retina and sclera samples were mounted onto glass slides using Mounting Fluorescence Medium (DAKO) and examined using an Axio Imager M2 fluorescence microscope and Zen lite 2012 software (Zeiss).

2.8. Statistical analysis

All results are given as mean (±SEM). Two-tail analysis of variance (ANOVA) and ratios were calculated of all experimental data obtained during the study. Statistically significant values are indicated by asterisks (* means $p < 0.05$, ** means $p < 0.01$, *** means $p < 0.001$).

3. Results

3.1. Computational enhancement of SLO recordings

Usage of *in vivo* data from FAF pictures of a conventional SLO for microglia identification and quantification is hampered by moving elements (e.g. monocytes), pixel noise and thus uncertain cell shape definition (Fig. 1A), the main discriminative criteria for the counting analysis. Image processing is the primary approach to

solve this problem. For that purpose we tested the proposed algorithms given in the Section 2.4. The criteria for selection of one processing algorithm were: a.) accuracy in microglia cell morphology assessment comparable to *ex vivo* analysis, b.) reduction of pixel noise and c.) removal of moving elements. The built-in image processing algorithm of the Heidelberg SLO reduces the pixel noise (comparing Fig. 1A and B) but neither enhances cell shape resolution nor removes transient elements. Performing frame averaging after recording, the image processing significantly eliminated mobile elements (Fig. 1C, black arrowhead) as well as image noise. This enhancement corrected the microglia phenotype before its analysis. Some cells which appeared as amoeboid before image processing looked clearly ramified afterwards. In long-duration videos, the refining result of the three algorithms was similar. However, when videos had a small amount of frames, LMedS and temporal median filter resulted in too low quality to clearly differentiate between the microglia morphologies. This was not the case with the frame averaging algorithm. Short videos are mandatory to keep experimental times as short as possible to diminish the duration of anesthesia and avoid corneal haze, which further reduces the quality of the images. Thus the two algorithms LMedS and temporal median filter, were discarded from further experiments.

The two major phenotypes that can be observed in the retina are the ramified, surveying microglia and the amoeboid, activated microglia (Langmann, 2007). *Ex vivo*, we were able to detect these two types of different activation by Iba-1 staining (Fig. 1D) indicating the reliable quality of the results obtained from frame averaging algorithm. The same features were observed *in vivo* by using SLO: ramified and amoeboid microglia (Fig. 1E). *In vivo*, we also detected a third type that we classified as intermediate between incipient and highly activated (Fig. 1E). For further analysis we considered the intermediate and the amoeboid types as activated microglia.

3.2. In vivo imaging of macrophages and microglia cells in the retina

The *in vivo* imaging of the retina was performed using a conventional scanning laser ophthalmoscope (SLO) (Fig. 2A). In the fundus auto-fluorescence mode or during fluorescence angiography, we were able to image microglia cells in MacGreen mice due to their EGFP signal (Fig. 2A, center and right, Video 1 and Video 2). Two major layers of stationary microglia were detected as it has been detailed in Section 2.3 and according to the schematic illustration (Fig. 2B, left panel). These two layers were the major ones containing both vessels and defined fluorescent macrophages. We identified these two layers as the inner and outer plexiform layers (IPL and OPL respectively; Fig. 1B, central and right panels), described in the literature as the layers that contain the major populations of microglia in the retina, and, at the same time, the major vessels (Xu et al., 2007). The localization of microglia populations and its matching with the fluorescence signal (EGFP) was verified *ex vivo* by co-staining of Iba-1, a commonly known marker for mononuclear phagocytes, and endogenously expressed GFP (Sasmono et al., 2003) in sagittal sections (Fig. 2C). The two cell populations (in the inner and the outer retina) found *in vivo* correspond to the two layers (IPL and OPL) verified *ex vivo*.

Supplementary video related to this article can be found at http://dx.doi.org/10.1016/j.exer.2015.07.012.

3.3. Analysis of microglia activation in laser-induced CNV

In order to show that our method enables the time-course analysis of macrophage activation, retinas were lasered as described above, placing 3 laser spots in one half of the eye and objected to SLO imaging at distinct time points after laser procedure (Fig. 3A). Based on the quantification of non-activated cells at the different time-points, we observed a slight increase in the amount of ramified cells among the time, only significant at D4 in the IPL (133 ± 15 cells per total fundus area of 0.7 mm^2, $p = 0.039$). Considering the analysis of activated cells in the outer layer (Fig. 3B, OPL), significant differences were only found at D4 (14 ± 2 cells per total fundus area; D4 respect to D1, $p = 0.041$). The major activation took place in the inner layer: one hour after laser treatment no active microglia was detected, whereas the turnover to an activated stage became evident at D1 (25 ± 5 cells per total fundus area; D1 respect to D0, $p = 0.017$). At this time point, we noticed predominantly the intermediate phenotype of microglia (Fig. 1E, right panel). At the following time-points this phenotype was no longer observed, turning the amoeboid phenotype to be the predominant one. The peak of activated cells was reached at D4 (39 ± 3 cells per total fundus area; D4 respect to D1, $p = 0.045$) which then decreased reaching significant reduced numbers at D7 (28 ± 4 cells per total fundus area; D7 respect to D4, $p = 0.047$) and sustained at D14 (32 ± 4 cells per total fundus area; D14 respect to D7, $p = 0.476$) (Fig. 3B, IPL). Calculating ratios of activated against not activated cells supported the significant increase in activated cells between D4 respect to D14 whereas the differences between D7 and D14 are not (data not shown).

To prove that the number of activated cells *in vivo* correlates with a quantification *ex vivo*, we determined the same analysis in retina whole-mounts at the end-point of the experiment, D14, using the mononuclear phagocyte marker CD11b (Ma et al., 2009). We found a correlation of the rates in activation (Suppl. Table 1). The distribution of cells was the same in our observation *ex vivo* and *in vivo*.

As the presence of activated cells was not limited to the area of laser impact, we compared the time-course of distribution of activated macrophages in the outer and the inner layer in both the treated and the non-treated parts of the retina (Fig. 3C). Calculating the ratio of activated cells in untreated side (half of the total fundus, 0.35 mm^2) versus laser side (the other half, 0.35 mm^2), we found that the levels of activated microglia in outer layer remained stable over the observation time. However, in the inner layer we observed a significant increase (D7 respect to D4, $p = 0.013$) in the ratios between activated and non-activated microglia, demonstrating that activation spreads all over the retina with time. In control eyes from untreated animals, we barely observed activated cells, and when that happened, it was always in the outer and never in the inner layer (data not shown).

We correlated the number of cells (both non-activated and activated) to the tissue damage. Damage was quantified as percentage of auto-fluorescent area among the total fundus area (Fig. 3B, Suppl. Fig. 1 A–B). At D0 after laser injury, the auto-fluorescent tissue was $3 \pm 0.3\%$ of the total fundus area visualized (0.7 mm^2). The peak in relative tissue damage was detected at D4 ($5.9 \pm 0.7\%$ of the total fundus area), decreasing to $2.8 \pm 0.5\%$ at D14. Again these *in vivo* data correlates with *in situ* observations: in sagittal sections, we found intense auto-fluorescence in the area belonging to the scar at D4 (Fig. 3D).

We correlated the SLO imaging results with *ex vivo* staining of mononuclear phagocytes with Iba-1 (Fig. 3D). By selecting sagittal sections containing the laser scar, both the localization of the mononuclear phagocytes and the disruption of the RPE were evaluated. The laser injury progressed from a small rupture at D1 to a disruption of the outer neural retina at D7. Abundant presence of Iba-1 positive cells was detected at the scar area from D4 on (Fig. 3D, black arrowheads) as well as in the neural retina, some of them migrating (Fig. 3D, white arrowheads).

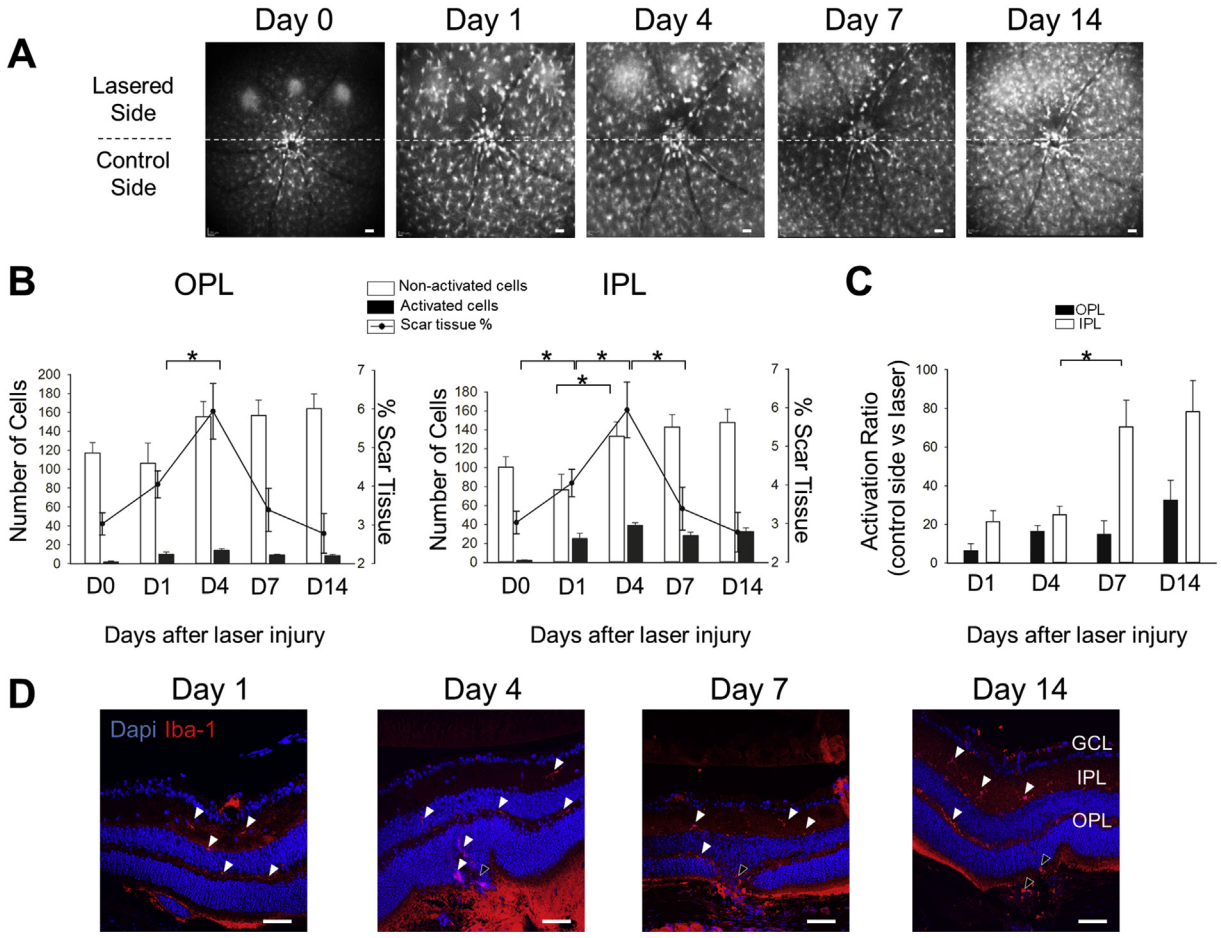

Fig. 3. Time-Course of Microglia Activation. A SLO auto-fluorescence images at selected time points after applying three laser spots on one half of the eye: D0, D1, D4, D7 and D14 showing differences in macrophage behavior. Scale bar represents 100 μm. B Bar chart (left axis) represents the mean value of counted cells in the total fundus area at selected time points in both IPL and OPL. Bars in white refer to non-activated cells and bars in black to the activated ones. The line (right axis) shows the percentage of auto-fluorescent scar tissue. All error bars represent SEM. (N = 5–6) C Analysis of the ratios of activated cells regarding their distribution in the not lasered (half of the fundus) versus lasered side (the other half) at OPL (black) and IPL (white) at selected time points. (N = 5) D Staining of sagittal sections of retina against Iba-1 (red) locating mononuclear phagocytes in the neural retina (white arrowheads) and in the vicinity of the scar (black arrowheads) at different time points: D1, D4, D7 and D14 at the laser scar area. Nuclei were counterstained by DAPI (blue). Scale bar represents 100 μm.

3.4. Laser power impact in microglia activation

The intensity of laser power was considered as one critical trigger for severity of microglia activation. In order to assess its physiological relevance, we compared the impact of 120 mW, an established power for inducing CNV in rodents, (Semkova et al., 2014) used in our previous experiments to a higher one of 240 mW. No obvious differences between both energies were detectable *in vivo* (Fig. 4A). Comparing the number of activated cells from SLO recording, we did not find significant differences at D7 respect to D4 ($p = 0.57$) and D14 respect D7 ($p = 0.053$) (Fig. 4C). Considering the peak of activation at D4 in the inner layer in our study, choroid whole-mount preparations showed no differences in CNV, and Iba-1 positive cells behaved similarly (Fig. 4B).

4. Discussion

In this study we provide evidence that conventional SLO can be used for reliable *in vivo* monitoring of temporal and spatial behavior of activated macrophages in a retinal neovascularization process. Post experimental image processing permitted safe identification and quantification of activated cells. Using this method we found new features of macrophage/microglia activation in response to laser injury: absence of an acute reaction, a transitory phenotype of microglia and involvement of activated microglia predominantly in the inner retina.

To approach translational research targeting microglia activation, transgenic mouse models which display either macrophage-specific (MacGreen) or microglia-specific ($CX3CR1^{GFP/+}$) GFP expression have successfully contributed to a better understanding of pathogenic mechanisms in retinal degeneration. *In vivo* analysis of microglia behavior might provide additional information required for defining therapeutic strategies. Using conventional SLO, the *in vivo* assessment of microglia activation in retinal degeneration was so far inconclusive due to the bad quality and resolution of the acquired pictures. The main reasons for the poor quality are moving elements (e.g. monocytes) and pixel noise leading to uncertain cell shape definition.

As SLO allows the visualization of all EGFP positive cells, some flowing cells might be wrongly captured during a static imaging as the focus of the camera stays on the vessels. Furthermore, the limitations of camera resolution produce considerable pixel noise. Spectralis HRA-OCT has its own frame averaging option while capturing images. This method performs the same processing as the averaging algorithm, but with the limitation of a maximum of 100 frames. Hereby not all the transient elements are removed and

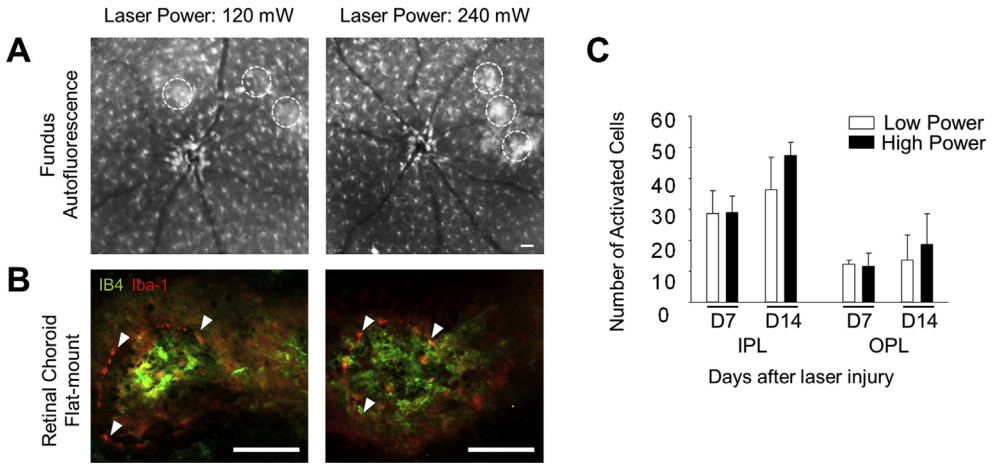

Fig. 4. Comparison of Time-Course of Microglia Activation at Different Laser Power. A SLO auto-fluorescence images focusing IPL at D4 lasered animal using different laser powers (120 and 240 mW). B Co-staining of retinal choroid flat-mount against IB4 (green) to show vessels and Iba-1 (red) pointing microglia sitting at the choroidal scar (marked with arrowheads). Staining was performed at D4 in lasered animals, comparing different laser power conditions. Bars represent 100 μm. C Bar chart represents the mean value of activated cells at different conditions of low laser power (120 mW, in white) and high laser power (240 mW, in yellow) at D7 and D14 in both the IPL and OPL. Error bars represent SEM. (N = 4–6).

some areas remain too noisy due to subtle movements of the animal. We addressed this problem by employing the offline frame averaging technique described in Section 2.4. The method of frame averaging from recorded videos allowed elimination of moving elements, such as monocytes, and reduction of pixel noise. Using that algorithm we could more reliably identify and classify the cells, and it can be applied on already processed Heidelberg videos obtaining a better resolution (Fig. 1B). In future, it might be interesting to investigate how diverse image processing techniques, such as histogram equalization and Otsu's adaptive threshold (Otsu, 1979), can further improve the manual and semi-automatic classification and quantification of microglia.

The uncertain identification of cell phenotypes, and thus their quantification, is a common problem using imaging methods. One might think about quantifying the fluorescence signal intensity. This, unfortunately, has two main problems: The first is that the laser intervention produces a basal auto-fluorescence that differs from spot to spot (Suppl. Fig. 1C). The second is that it is not possible to use a standard exposure during the measurements as not all the samples present optimal conditions for imaging (Bell et al., 2014; Bermudez et al., 2011; Calderone et al., 1986; Ridder et al., 2002). Because of these reasons, using a quantification based on phenotype provides us more reliable information. To select the appropriate algorithm for that purpose, the following criteria, in addition to those described above, were applied: accuracy of cell morphology identification compared to *ex vivo* analysis and minimal acquisition time. We selected the frame averaging algorithm because its output was the most optimal with the smallest number of frames.

In addition to identification of cell morphology, the EGFP-fluorescent cells can be also localized in two different layers. Using the focus strategies described in Section 2.3, scanning through the tissue *in vivo*, one layer was assigned close to the photoreceptors, while the other one was in the inner retina. Sagittal sections of the retina, stained against Iba-1 as a marker for microglia cells (Chen et al., 2015; Howlett et al., 2011; Imai et al., 1996; Karlstetter et al., 2014; Rojas et al., 2014; Wang et al., 2013; Xu et al., 2007), revealed that all GFP positive cells are also Iba-1 positive and exclusively merge in the inner and outer layers of the retina. Although the *in situ* confirmation of *in vivo* data has already been reported by other groups (Alt et al., 2014; Eter et al., 2008; Joly et al., 2009; Xu et al., 2008), the *in vivo* assignment of the mononuclear phagocytes to the two layers was so far not accomplished by others.

The activation of microglia in retinal degenerative processes includes both the morphology switch from ramified to amoeboid phenotype and the change in spatial distribution (Langmann, 2007). Using laser-induced CNV we observed the transition from ramified to amoeboid phenotype and the change of cell distribution in relation to the side of laser impact. These phenotypes are clearly distinguished *ex vivo* in retina whole-mounts. In FAF, a third phenotype could be observed, representing an intermediate state between the ramified and the amoeboid one. That one could not be recognized *ex vivo*. The fixation procedure for immunodetection might render the detection of subtle changes in cell shape impossible. Nevertheless, the physiological role of activated microglia in general but also that of microglia displaying the intermediate phenotype requires further *in situ* analysis.

The follow-up investigation of microglia by FAF revealed surprising aspects of microglia activation after laser-injury. One hour after laser-treatment, no acute reaction was detected. That was also observed by Eter (Eter et al., 2008), although they found a shorter period of latency. It needs to be mentioned that Eter et al. did not use enhanced image analysis. After 24 h, an increase in the number of activated microglia was manifest. The peak of activation was detected at D4 after laser treatment which decreased at D7 and was sustained at D14. Astonishingly, the majority of activated cells was found in the inner retina whereas the laser scar is located at the outer retina (Guthrie et al., 2014). Most of the cells counted at D1 were found surrounding the scar. After D4 we observed a spreading of the activated cells reaching a homogenous distribution at D14 in the inner retina. This observation might be biased by the fact that activated cells were only counted at lesion sides and not in relation to untreated sides, which might also contain activated cells especially when comparing IPL and OPL. Thus we extended the analysis towards calculating the ratios of activated cells in untreated versus laser-treated sides. The ratio increased most significantly in IPL at D7 and D14 and not at D4. This indicates that at D7 not only the total number has increased but now also activated cells are more homogenously distributed and not exclusively concentrated in laser-treated areas. To our knowledge, the overall activation of microglia in the inner and not in the outer retina, where the laser scar is present, has not been analyzed and shown so far. We suggest

that microglia subpopulations in the retina have a highly defined role which is still not well understood. Thus the inner retina microglia subpopulation might have a predefined and specific protective role against retinal damage. Although lacking a concrete mechanism, this finding could have an impact for the safety and clinical relevance of low threshold laser treatments such as in diabetic retinopathy (Luttrull et al., 2005).

When correlating the number of activated microglia to the tissue damage taken as auto-fluorescent tissue, we found that the major leap in the number coincided with the peak of auto-fluorescent tissue. Given the fact that we did not observe an acute reaction, this coincidence might help to better understand mechanisms of microglia activation, which are beyond the scope of this study.

The laser power to elicit CNV might affect the strength of reaction of microglia. Since we didn't detect any acute reaction one hour after laser treatment, we doubled the power in order to provoke a faster and stronger response. Under these conditions we were not able to perform *in vivo* analysis as the treatment caused an increase in the opacity of the cornea until D4. However, the quantification of activated cells at D7 and D14 showed the same pattern of spatial and temporal distribution of activated microglia. Interestingly, we found no differences in the quantity of activated microglia cells between the moderate and the severe laser power. Analyzing the choroid *ex vivo*, we tracked mononuclear phagocytes using Iba-1, detecting their migration out of the neural retina (Combadiere et al., 2007), showing similar behavior in both laser treatments. This is supported by other works, where it is shown that, independent of the retinal and RPE damage, Iba-1 positive cells are attracted to the injured area (Muther et al., 2010).

In summary, this study provides evidence that conventional SLO can be used for *in vivo* analysis of microglia activity in the degenerating retina by comparing *in situ* and *in vivo* data. Our study highlights that image processing is required for accurate identification of the functional microglia phenotype. Moreover it even enables the detection of phenotypes which cannot be observed in immunohistochemistry probably due to the fixation methods. However, a large number of questions cannot be answered by SLO imaging. Furthermore, the activated microglia are known to display a large variety of functional phenotypes which all have the same morphological phenotype (Murray et al., 2014). Thus even advanced *in vivo* imaging requires *in situ* verification and additional information about cellular behavior and molecular classification of their functional phenotype.

Acknowledgments and funding source

Authors thank Polykarpos Karamaounas for technical assistance in the digital processing of images, Anna-Karina Maier and Sergej Skosyrski for teaching laser and SLO imaging techniques and Thomas Langmann from University of Cologne for his scientific advice.

This research was made possible by a Marie Curie grant from the European Commission in the framework of the REVAMMAD ITN (Initial Training Research network), Project number 316990 and Deutsche Forschungsgemeinschaft grant DFG Jo 324/10-1 and 10-2.

Appendix A. Supplementary data

Supplementary data related to this article can be found at http://dx.doi.org/10.1016/j.exer.2015.07.012.

References

Alt, C., Runnels, J.M., Mortensen, L.J., Zaher, W., Lin, C.P., 2014. In vivo imaging of microglia turnover in the mouse retina after ionizing radiation and dexamethasone treatment. Invest. Ophthalmol. Vis. Sci. 55, 5314–5319.

Bell, B.A., Kaul, C., Hollyfield, J.G., 2014. A protective eye shield for prevention of media opacities during small animal ocular imaging. Exp. Eye Res. 127, 280–287.

Bermudez, M.A., Vicente, A.F., Romero, M.C., Arcos, M.D., Abalo, J.M., Gonzalez, F., 2011. Time course of cold cataract development in anesthetized mice. Curr. Eye Res. 36, 278–284.

Calderone, L., Grimes, P., Shalev, M., 1986. Acute reversible cataract induced by xylazine and by ketamine-xylazine anesthesia in rats and mice. Exp. Eye Res. 42, 331–337.

Chambers, S.E., O'Neill, C.L., O'Doherty, T.M., Medina, R.J., Stitt, A.W., 2013. The role of immune-related myeloid cells in angiogenesis. Immunobiology 218, 1370–1375.

Chen, X., Zhou, H., Gong, Y., Wei, S., Zhang, M., 2015. Early spatiotemporal characterization of microglial activation in the retinas of rats with streptozotocin-induced diabetes. Graefe's archive for clinical and experimental ophthalmology = Albrecht von Graefes Archiv fur klinische und experimentelle Ophthalmologie 253, 519–525.

Combadiere, C., Feumi, C., Raoul, W., Keller, N., Rodero, M., Pezard, A., Lavalette, S., Houssier, M., Jonet, L., Picard, E., Debre, P., Sirinyan, M., Deterre, P., Ferroukhi, T., Cohen, S.Y., Chauvaud, D., Jeanny, J.C., Chemtob, S., Behar-Cohen, F., Sennlaub, F., 2007. CX3CR1-dependent subretinal microglia cell accumulation is associated with cardinal features of age-related macular degeneration. J. Clin. Invest. 117, 2920–2928.

Contag, C.H., Bachmann, M.H., 2002. Advances in in vivo bioluminescence imaging of gene expression. Annu. Rev. Biomed. Eng. 4, 235–260.

Edinger, M., Cao, Y.A., Hornig, Y.S., Jenkins, D.E., Verneris, M.R., Bachmann, M.H., Negrin, R.S., Contag, C.H., 2002. Advancing animal models of neoplasia through in vivo bioluminescence imaging. Eur. J. Cancer 38, 2128–2136.

Eter, N., Engel, D.R., Meyer, L., Helb, H.M., Roth, F., Maurer, J., Holz, F.G., Kurts, C., 2008. In vivo visualization of dendritic cells, macrophages, and microglial cells responding to laser-induced damage in the fundus of the eye. Invest. Ophthalmol. Vis. Sci. 49, 3649–3658.

GmbH, H.E., 2007. Spectralis Hardware Operating Instructions. Heidelberg Engineering.

Grisanti, S., Tatar, O., 2008. The role of vascular endothelial growth factor and other endogenous interplayers in age-related macular degeneration. Prog. Retin. Eye Res. 27, 372–390.

Guthrie, M.J., Osswald, C.R., Valio, N.L., Mieler, W.F., Kang-Mieler, J.J., 2014. Objective area measurement technique for choroidal neovascularization from fluorescein angiography. Microvasc. Res. 91, 1–7.

Hanisch, U.K., Kettenmann, H., 2007. Microglia: active sensor and versatile effector cells in the normal and pathologic brain. Nat. Neurosci. 10, 1387–1394.

Howlett, D.R., Bate, S.T., Collier, S., Lawman, A., Chapman, T., Ashmeade, T., Marshall, I., Anderson, P.J., Philpott, K.L., Richardson, J.C., Hille, C.J., 2011. Characterisation of amyloid-induced inflammatory responses in the rat retina. Exp. Brain Res. 214, 185–197.

Huang, T.S., Hsu, Y.P., 1981. Image sequence enhancement. In: Huang, P.T.S. (Ed.), Image Sequence Analysis, Springer Series in Information Sciences, pp. 289–309.

Imai, Y., Ibata, I., Ito, D., Ohsawa, K., Kohsaka, S., 1996. A novel gene iba1 in the major histocompatibility complex class III region encoding an EF hand protein expressed in a monocytic lineage. Biochem. Biophys. Res. Commun. 224, 855–862.

Joly, S., Francke, M., Ulbricht, E., Beck, S., Seeliger, M., Hirrlinger, P., Hirrlinger, J., Lang, K.S., Zinkernagel, M., Odermatt, B., Samardzija, M., Reichenbach, A., Grimm, C., Reme, C.E., 2009. Cooperative phagocytes: resident microglia and bone marrow immigrants remove dead photoreceptors in retinal lesions. Am. J. Pathol. 174, 2310–2323.

Karlstetter, M., Nothdurfter, C., Aslanidis, A., Moeller, K., Horn, F., Scholz, R., Neumann, H., Weber, B.H., Rupprecht, R., Langmann, T., 2014. Translocator protein (18 kDa) (TSPO) is expressed in reactive retinal microglia and modulates microglial inflammation and phagocytosis. J. Neuroinflammation 11, 3.

Langmann, T., 2007. Microglia activation in retinal degeneration. J. Leukoc. Biol. 81, 1345–1351.

Luttrull, J.K., Musch, D.C., Mainster, M.A., 2005. Subthreshold diode micropulse photocoagulation for the treatment of clinically significant diabetic macular oedema. Br. J. Ophthalmol. 89, 74–80.

Ma, W., Zhao, L., Fontainhas, A.M., Fariss, R.N., Wong, W.T., 2009. Microglia in the mouse retina alter the structure and function of retinal pigmented epithelial cells: a potential cellular interaction relevant to AMD . PloS one 4, e7945.

Murray, P.J., Allen, J.E., Biswas, S.K., Fisher, E.A., Gilroy, D.W., Goerdt, S., Gordon, S., Hamilton, J.A., Ivashkiv, L.B., Lawrence, T., Locati, M., Mantovani, A., Martinez, F.O., Mege, J.L., Mosser, D.M., Natoli, G., Saeij, J.P., Schultze, J.L., Shirey, K.A., Sica, A., Suttles, J., Udalova, I., van Ginderachter, J.A., Vogel, S.N., Wynn, T.A., 2014. Macrophage activation and polarization: nomenclature and experimental guidelines. Immunity 41, 14–20.

Muther, P.S., Semkova, I., Schmidt, K., Abari, E., Kuebbeler, M., Beyer, M., Abken, H., Meyer, K.L., Kociok, N., Joussen, A.M., 2010. Conditions of retinal glial and inflammatory cell activation after irradiation in a GFP-chimeric mouse model. Invest. Ophthalmol. Vis. Sci. 51, 4831–4839.

Otsu, N., 1979. Threshold selection method from gray-level histograms. IEEE Trans. Syst. Man Cybern. 9, 62–66.

Ridder 3rd, W., Nusinowitz, S., Heckenlively, J.R., 2002. Causes of cataract development in anesthetized mice. Exp. Eye Res. 75, 365–370.

Rojas, B., Gallego, B.I., Ramirez, A.I., Salazar, J.J., de Hoz, R., Valiente-Soriano, F.J., Aviles-Trigueros, M., Villegas-Perez, M.P., Vidal-Sanz, M., Trivino, A., Ramirez, J.M., 2014. Microglia in mouse retina contralateral to experimental glaucoma exhibit multiple signs of activation in all retinal layers. J. Neuroinflammation 11, 133.

Rousseeuw, P.J., Leroy, A.M., 1984. Robust Regression and Outlier Detection. John Wiley, New York.

Rudin, M., Weissleder, R., 2003. Molecular imaging in drug discovery and development. Nat. Rev. Drug Discov. 2, 123–131.

Sasmono, R.T., Oceandy, D., Pollard, J.W., Tong, W., Pavli, P., Wainwright, B.J., Ostrowski, M.C., Himes, S.R., Hume, D.A., 2003. A macrophage colony-stimulating factor receptor-green fluorescent protein transgene is expressed throughout the mononuclear phagocyte system of the mouse. Blood 101, 1155–1163.

Semkova, I., Kociok, N., Karagiannis, D., Nischt, R., Smyth, N., Paulsson, M., Strauss, O., Joussen, A.M., 2014. Anti-angiogenic effect of the basement membrane protein nidogen-1 in a mouse model of choroidal neovascularization. Exp. Eye Res. 118, 80–88.

Stoecker, K., Weigelt, K., Ebert, S., Karlstetter, M., Walczak, Y., Langmann, T., 2009. Induction of STAP-1 promotes neurotoxic activation of microglia. Biochem. Biophys. Res. Commun. 379, 121–126.

Wang, N.K., Lai, C.C., Liu, C.H., Yeh, L.K., Chou, C.L., Kong, J., Nagasaki, T., Tsang, S.H., Chien, C.L., 2013. Origin of fundus hyperauto-fluorescent spots and their role in retinal degeneration in a mouse model of Goldmann-Favre syndrome. Dis. Model Mech. 6, 1113–1122.

Witmer, A.N., Vrensen, G.F., Van Noorden, C.J., Schlingemann, R.O., 2003. Vascular endothelial growth factors and angiogenesis in eye disease. Prog. Retin. Eye Res. 22, 1–29.

Xu, H., Chen, M., Manivannan, A., Lois, N., Forrester, J.V., 2008. Age-dependent accumulation of lipofuscin in perivascular and subretinal microglia in experimental mice. Aging Cell 7, 58–68.

Xu, H., Chen, M., Mayer, E.J., Forrester, J.V., Dick, A.D., 2007. Turnover of resident retinal microglia in the normal adult mouse. Glia 55, 1189–1198.

Curriculum vitae

My curriculum vitae does not appear in the electronic version of my thesis for reasons of data protection.

Curriculum vitae

My curriculum vitae does not appear in the electronic version of my thesis for reasons of data protection.

Curriculum vitae

My curriculum vitae does not appear in the electronic version of my thesis for reasons of data protection.

Curriculum vitae

My curriculum vitae does not appear in the electronic version of my thesis for reasons of data protection.

Complete list of publications

Peer-reviewed journal papers:

Reichhart N, Haase N, **Crespo-Garcia S**, Skosyrski S., Herrspiegel C, Kociok N, Fuchshofer R, Dillinger A, Poglitsch M, Muller DN, Joussen AM, Luft FC, Dechend R, Strauss O. (**2016**) Hypertensive Retinopathy in a Transgenic Angiotensin-based Model. Clinical science [*Epub ahead of print*]

Kociok N, **Crespo-Garcia S**, Liang Y, Klein SV, Nürnberg C, Reichhart N, Skosyrski S, Moritz E, Maier AK, Brunken WJ, Strauß O, Koch M, Joussen AM. (**2016**) Lack of netrin-4 modulates pathologic neovascularization in the eye. Scientific reports 6: 18828

Crespo-Garcia S, Reichhart N, Hernandez-Matas C, Zabulis X, Kociok N, Brockmann C, Joussen AM, Strauss O. (**2015**) In vivo analysis of the time and spatial activation pattern of microglia in the retina following laser-induced choroidal neovascularization. Experimental eye research 139: 13-21

Reichhart N, Markowski M, Ishiyama S, Wagner A, **Crespo-Garcia S**, Schorb T, Ramalho JS, Milenkovic VM, Fockler R, Seabra MC, Strauss O. (2015) Rab27a GTPase modulates L-type Ca2+ channel function via interaction with the II-III linker of CaV1.3 subunit. Cellular signalling 27: 2231-2240

Martin-Mateos P, **Crespo-Garcia S**, Ruiz-Llata M, Lopez-Fernandez JR, Jorcano JL, Del Rio M, Larcher F, Acedo P. (**2014**) Remote diffuse reflectance spectroscopy sensor for tissue engineering monitoring based on blind signal separation. Biomedical optics express 5: 3231-3237

Conference papers:

Martín-Mateos P, **Crespo-Garcia S**, Ruiz-Llata M, Lopez-Fernandez JR, Jorcano JL, Del Rio M, Larcher F, Acedo P. (2014) Portable, Non-contact, Diffuse Reflectance Spectroscopy System for Early Skin Implants Assessment, Biomedical Optics. Optical Society of America, p. BS3A. 40.

Acknowledgements

I would like to express my most sincere gratitude to my supervisor in this work, Prof. Antonia M Joussen, from who I have learnt to be passionate in understanding retinal vascular disease in a very translational manner. With her wise guidance and support I have grown as scientist and researcher during the last years, and thanks to her I am keen to continue developing my career in Ophthalmology.

Equally, I need to show gratitude to, my also supervisor, Prof. Olaf Strauß. Gratitude to his daily presence in my research routine, our long conversations about Science and rowing, and especially, to his questions. Thank you for keeping your door always open.

Besides my supervisors, I would like to thank the scientists which work force and human beings I profoundly admire, that agreed to join the rest of my thesis committee: Prof. Alan Stitt, Dr. Florian Sennlaub, Prof. Antje Grosche, Prof. Frank Heppner and Prof. Uwe Pleyer. Since I have develop my –still– short career reading and learning from their work, I feel honored that they can now judge mine here with their insightful comments.

During the development of my doctorate I had the chance to establish great connections and collaborative partnerships. Firstly, with Queen's University of Belfast (Centre for Experimental Medicine), where Prof. Alan Stitt and Prof. Heping Xu, together with their fantastic teams, helped me in the achievement of new techniques and insights in the field of retinal disease. Secondly, I am thankful also to the interdisciplinary collaboration with Carlos Hernández-Matas and Dr. Xenophon Zabulis and their team in FORTH (Institute of Computer Science) in Crete and all the people within the REVAMMAD European consortium.

My sincere thanks also goes to Dr Nadine Reichhart, my partner in eternal scientific –and random– discussion, and Dr Norbert Kociok, office mate and mentor in all concerns of animal experimentation. Thank you both too for your part-time work as translators.

A special mention to Gabriele Fels and Sergej Skosyrski for their help in acquiring the lab techniques and keeping organized all logistics.

I thank my fellow labmates and medical doctors from the clinic upstairs (and in Steglitz) for all the horrible filter coffee shared in the lab, and the small talk that made work easier.

Quiero dar las gracias a todos mis mentores pasados que, de una manera u otra, han contribuido a que sea cómo soy y que me siga apasionando la ciencia.

Mi gracias más afectuoso es para mi familia, por su desinteresado apoyo moral y cariño a lo largo de estos años, pues solo ellos me han visto evolucionar en todo su proceso. Y aunque no todos están aquí, sé que ellos están orgullosos.

A mis amigos, que no son sino la familia que yo he escogido, y sin los cuales mi vida sería insípida. Vosotros sois mi fuerza.

Y dejo para el final mi eterna gratitud al amor de mi vida, en estos momentos en Roma, pero siempre presente. Porque ella es quien me hace dar lo mejor de mí en cada singular aspecto de mi vida.